The 8th European Congress on Computational Methods in Applied Sciences and Engineering
ECCOMAS Congress 2022
5-–9 June 2022, Oslo, Norway

ON THE CONSERVATION OF PRIMARY AND SECONDARY PROPERTIES IN THE SIMULATION OF MULTIPHASE FLOWS

N. Valle[1*], F.X. Trias[2] and R.W.C.P Verstappen[1]

[1] Bernoulli Institute, University of Groningen, PO Box 407, 9700AK Groningen, The Netherlands, n.valle.marchante@rug.nl, r.w.c.p.verstappen@rug.nl

[2] Heat and Mass Transfer Technological Center, Technical University of Catalonia C/Colom 11, 08222 Terrassa (Barcelona), francesc.xavier.trias@upc.edu

Key words: multiphase flows, symmetry-preserving, discrete conservation properties, spurious currents

Abstract. The formulation of multiphase flows emanates from basic conservation laws: mass, momentum and energy. While these are embedded in the celebrated Navier-Stokes equations, none of these properties do necessarily hold when constructing a computational model, unless special care is taken in discretizing the different terms of the governing equations. The conservation of both primary (mass, momentum) and secondary (energy) quantities is not only relevant to mimic the dynamics of the system, but also computationally beneficial. Conservation of such quantities produce an enhanced physical reliability, removing most of the need for stabilization artifacts. In addition, discrete conservation implies numerical stability as well, producing inherently stable problems.

Focusing on the capillary force, which is one of the most distinguishable features of multiphase flows, we present here our most recent developments in the quest for conservation. Departing from an inherently mass conservative method, in this work we sketch our previous developments to obtain an energy conservation and next we present our attempt at momentum. By carefully assessing the continuum formulation, we delve into the mathematical properties responsible for the conservation of linear momentum, which we then mimic in the regularized and discrete formulations.

1 INTRODUCTION

Bubbly flow technologies are ubiquitous in industry. Example applications range from drag reduction around ship hulls [1] to tuning chemical selectivity in process industry [2], among others [3]. However, the development of these technologies firstly requires advancing our knowledge of the physical mechanisms ruling bubble dynamics [3].

A common thread behind most of the aforementioned technologies is the modification of large scale (flow) features by means of small scale (i.e., bubbles) ones [4, 5]. Two of the most relevant mechanisms in bubble flow technology are buoyancy, arising from the uneven density of the dispersed and continuous phase; and wake damping, due to the elastic deformation of the bubble interface by surface tension. Other important phenomena are bubble coalescence

in phase-change applications (e.g., boiling, electrolysis), and bubble break-up in atomization processes (e.g., combustion, spray coating) which are also due to surface tension. All these contribute to modify the flow features, like its turbulent spectra [6].

The incompressible Navier-Stokes equations describe such flows in most industrially relevant conditions. These state the conservation of mass and momentum explicitly, which are regarded as primary invariants; they also state the conservation of mechanical energy (in the abscence of viscosity) implicitly, which is regarded as a secondary (inviscid) invariant. Their solution contains the description of all the aforementioned flow features.

The lack of an analytic solution, the small characteristic length scale at which these process happen, together with its delicate nature, render Direct Numerical Simulation (DNS) as an essential tool to gain understanding on its ruling physics. DNS aims at representing the governing equations directly (i.e., the Navier-Stokes equations), without taking any further modeling assumptions on the solution. Our *leitmotiv* is that, as far as the physical setup is stable, so should the numerical one. Not only that, but it should attain stability by mimicking the same physical mechanisms in charge of such stability. It can be proven that the conservation of those corresponds with both a guaranteed stability and an improved physical reliability. This has proven to be invaluable in the DNS of turbulent flows [7, 8].

However, the DNS of multiphase flows is slightly less developed that its single-phase counterpart, precisely because of the even more complex interplay of different length scales [9]. In particular, the inclusion of very high liquid-gas density ratios and/or surface tension typically leads to numerical instabilities [10]. To address such instabilities, it is a common trend the addition of artificial damping mechanisms which, most critically in the context of turbulence, compromises the physical reliability of the model [11]. On the contrary, in the spirit of the DNS, our aim is to compute a numerical solution that mimics the continuum one in terms of the (discrete) conservation of basic quantities: mass, momentum and energy.

The conservation of both primary and secondary invariants is beneficial for the quality of the simulation because of twofold reason: (i) from the numerical perspective, the conservation of energy implies stability of the discrete system. This guarantees that the solution will eventually attain a stable solution. Then, (ii) from the physical perspective, the discrete conservation laws are exactly satisfied. This provides with an enhanced seal of quality to the output of the simulations.

Previous attempts on the conservation have obtained limited success, and to the best of our knowledge no methods has been able to simultaneously attain the conservation of mass, momentum and energy at the discrete level. While the conservation of mass is straightforward for the Volume Of Fluid (VOF) [12], Phase Field (PF) [13] and the Conservative Level Set (CLS) [14] methods, the conservation of linear momentum and mechanical energy has seen much limited progress. These include the conservation of energy for PF [15, 16], VOF [17] (partially), and most recently CLS [18] methods; while the conservation of linear momentum has seen limited success to 2D situations [19].

The main difficulty on the conservation of linear momentum and mechanical energy stems from the inclusion of surface tension [10]. In turn, this strongly depends on how the interface is represented at the discrete level. In this regard, the use of regularized (i.e., diffuse) interfaces results into a mathematically better posed problem [20, 18].

In this paper, we discuss our present efforts in the development of a fully conservative numer-

ical method for multiphase flows. Departing form our recent developments [18] in the context of the CLS, we review the analytic, regularized and (when possible) discrete formulations leading to the conservation of linear momentum and mechanical energy.

2 CONTINUUM FORMULATION

The dynamics of multiphase flows is accurately represented by the incompressible Navier-Stokes equations. In their conservative form, they read:

$$\frac{\partial \rho \vec{u}}{\partial t} + \nabla \cdot (\rho \vec{u} \otimes \vec{u}) = \nabla \cdot \sigma \qquad\qquad \nabla \cdot \vec{u} = 0 \tag{1}$$

where ρ is density, $\vec{u}$ is the velocity field and σ is the stress tensor. The latter is composed of the hydrostatic and the deviatoric ones ($\sigma = -p\mathbb{I} + \tau$). Assuming that he flow is Newtonian, τ is defined by the Stokes constitutive equation $\tau = 2\mu S$, where the strain tensor is the symmetric part of $\nabla \vec{u}$, $S = 1/2\left(\nabla \vec{u} + (\nabla \vec{u})^T\right)$.

However, in the presence of tensile surfaces, the stress tensor σ presents a discontinuity. The reason behind it is the uneven molecular activity in the two phases across the interface, Γ. This induces a force parallel to the interface [21]. Across curved interfaces, this results into a stress discontinuity in the normal direction of the interface surface. As a result, the stress tensor includes the following discontinuity:

$$[\sigma]_\Gamma \, \hat{\eta}_i = -\gamma \kappa \hat{\eta}_i \tag{2}$$

where $\hat{\eta}_i$ is the interface normal, γ is the surface tension coefficient and κ is the interface curvature.

Owing to the conservative nature of equation (1), linear momentum is conserved in this formulation, while the conservation of mechanical energy has been extensively reported in the absence of discontinuities (see, e.g., [22]). Nonetheless, we will report next on the conservation of the both linear momentum and mechanical energy due to the stress discontinuity.

2.1 Energy

For the conservation of mechanical energy, we briefly summarize the procedure described in [18], by focusing solely on the contributions to the energy balance of the surface tension term. For a comprehensive detail of how the rest of the terms cancel each other, the interested reader is referred to [23, 18]. First, we introduce the mechanical energy as the sum of kinetic and surface energy.

$$\frac{dE_m}{dt} = \frac{dE_k}{dt} + \frac{dE_p}{dt} \tag{3}$$

The contributions to kinetic energy read as

$$\frac{dE_k}{dt} = \gamma \int_\Gamma \kappa \vec{u} \cdot \hat{\eta}_i dA \tag{4}$$

where dA stands for a differential control surface of the interface. Note that we have assumed that γ is constant. This accounts for the change of energy of the fluid due to the accelerating/stopping

effect of surface tension. On the other hand, the contribution to potential energy is due to the variation in Helmholtz's free energy, which reads as

$$\frac{dE_p}{dt} = \gamma \frac{d}{dt} \int_\Gamma dA \tag{5}$$

and contains the elastic energy stored in a tensile interface due to its deformation, in what can be seen as a 2D counterpart of the well-known 1D elastic energy of a spring. Overall, the entire system can be seen as a 3D counterpart of the well-known spring-mass system.

Introducing the first variation of area [24],

$$\frac{d}{dt} \int_\Gamma dA = - \int_\Gamma \kappa \vec{u} \cdot \hat{\eta}_i dA \tag{6}$$

which relates the evolution of surface area with its curvature times its normal velocity, we can prove that:

$$\frac{dE_m}{dt} = 0 \tag{7}$$

2.2 Linear momentum

For the conservation of linear momentum, the integral of the mean curvature vector, $\kappa \hat{\eta}_i$ [25]:

$$\int_\Gamma \kappa \hat{\eta}_i dA + \int_{\partial\Gamma} \hat{\eta}_i \times d\hat{\eta}_i = \vec{0} \tag{8}$$

states that for a closed surface (i.e., $\partial\Gamma = \emptyset$) momentum is conserved. It also states that, in case of an open surface the contribution of contact angle to the total momentum equation is introduced by means of the second term of equation (8). However, as a first attempt, we will disregard here the contact angle effect and focus on closed surfaces.

The continuum formulation has proven the conservation of mass and momentum and energy.

3 REGULARIZED FORMULATION

The use of a sharp representation of the interface poses several regularity issues, which become problematic at the computational stage. To overcome these, we consider the embedding of the different phases and the interface separating them into the ambient space and introduce a proper regularization. Following our previous work [18], we show that such a regularization is compatible with the first variation of area (6) as well as the integral of the mean curvature vector (8). The latter represents the main novelty of this work.

We introduce a smooth marker function, θ, as in the Conservative Level Set (CLS) method [14], which considers a smooth volume fraction, i.e.,: $\theta = 0$ correspond to one phase and $\theta = 1$ corresponds to the other one.

$$H(r) \approx \theta(r) = \frac{1}{2} \left(tanh \left(\frac{r}{2\epsilon} \right) + 1 \right) \tag{9}$$

where H is Heaviside's step function, r is the signed distance function of an arbitrary point in space to the interface, and ϵ controls the smearing of the profile. Note that as $\epsilon \to 0$, θ collapses

to the Heaviside step function $\theta \rightarrow H(r)$, which corresponds with the sharp representation of the interface used in Section 2 The interface surface is then reconstructed as in the Continuum Surface Force (CSF) method [26]

$$dA = |\nabla\theta| dV \qquad \hat{\eta}_i = \frac{\nabla\theta}{|\nabla\theta|} \qquad \kappa = \nabla \cdot \hat{\eta}_i \tag{10}$$

Finally, the marker function allows to replace the transport of the interface by the transport of a scalar, which is a much more amenable problem.

$$\frac{\partial\theta}{\partial t} + (\vec{u} \cdot \nabla)\theta = 0 \tag{11}$$

3.1 Energy

For the conservation of energy, we succinctly summarize the derivation described in [18] to show that the regularization introduced in equation (9), is compatible with the first variation of area (6). By using the surface reconstruction in (10) and the transport of the marker function (11), we arrive at

$$\frac{d}{dt}\int_\Gamma dA \approx \int_\Omega \hat{\eta}_i \cdot \nabla((\vec{u} \cdot \nabla)\theta) dV = \int_\Omega (\nabla \cdot \hat{\eta}_i)(\vec{u} \cdot \nabla)\theta dV \approx -\int_\Gamma \kappa \vec{u} \cdot \hat{\eta}_i dA \tag{12}$$

which proves that the use of a regularized marker function is compatible with the conservation of (regularized) energy. Details on the exact derivation can be found in [18].

3.2 Linear momentum

The next step is to show that the regularized surface tension term given in Eq.(10) preserves linear momentum re-writing it as a linear combination of terms that are in conservative form (divergence or gradient). To do so, we firstly apply the chain rule to both $\nabla|\nabla\theta|$ and $\nabla \cdot (\hat{\eta}_i \otimes \nabla\theta)$

$$\nabla|\nabla\theta| = \nabla(\hat{\eta}_i \cdot \nabla\theta) = (\hat{\eta}_i \cdot \nabla)\nabla\theta + \nabla\hat{\eta}_i \cdot \nabla\theta, \tag{13}$$

$$\nabla \cdot (\hat{\eta}_i \otimes \nabla\theta) = (\hat{\eta}_i \cdot \nabla)\nabla\theta + (\nabla \cdot \hat{\eta}_i)\nabla\theta, \tag{14}$$

then, re-arranging terms leads to

$$(\nabla \cdot \hat{\eta}_i)\nabla\theta \overset{Eq.14}{=} \nabla \cdot (\hat{\eta}_i \otimes \nabla\theta) - (\hat{\eta}_i \cdot \nabla)\nabla\theta \overset{Eq.13}{=} \nabla \cdot (\hat{\eta}_i \otimes \nabla\theta) - \nabla(\hat{\eta}_i \cdot \nabla\theta) + \nabla\hat{\eta}_i \cdot \nabla\theta. \tag{15}$$

Hence, it is clear that the net contribution to linear momentum exactly vanishes if the tensor $\nabla\hat{\eta}_i$ and the vector $\nabla\theta$ are orthogonal, i.e. $\nabla\hat{\eta}_i \cdot \nabla\theta = \vec{0}$. To show this, it suffices to prove it for the x-direction. Namely, recalling the definition of $\hat{\eta}_i = \nabla\theta/|\nabla\theta|$ and $|\nabla\theta| = \sqrt{\nabla\theta \cdot \nabla\theta}$, and applying the chain rule twice leads to

$$\frac{\partial}{\partial x}\left(\frac{\nabla\theta}{|\nabla\theta|}\right) = \frac{\partial_x(\nabla\theta)|\nabla\theta| - \nabla\theta\partial_x|\nabla\theta|}{|\nabla\theta|^2} = \frac{\partial_x(\nabla\theta)|\nabla\theta| - \nabla\theta(\partial_x(\nabla\theta) \cdot \nabla\theta)/|\nabla\theta|}{|\nabla\theta|^2}, \tag{16}$$

then, taking the dot product with $\nabla\theta$ and re-arraging terms yields

$$\frac{\partial}{\partial x}\left(\frac{\nabla\theta}{|\nabla\theta|}\right) \cdot \nabla\theta = \frac{|\nabla\theta|(\partial_x(\nabla\theta) \cdot \nabla\theta) - |\nabla\theta|^2/|\nabla\theta|(\partial_x(\nabla\theta) \cdot \nabla\theta)}{|\nabla\theta|^2} = 0, \tag{17}$$

showing that vectors $\partial_x(\nabla\theta/|\nabla\theta|)$ and $\nabla\theta$ are orthogonal. Applying the same reasoning to other spatial direction leads to the following orthogonality relation

$$\nabla\hat{\eta}_i \cdot \nabla\theta = \vec{0}. \tag{18}$$

Finally, combining Eqs.(13), (15) and (18) leads to the following conservative form for the regularized surface tension term

$$(\nabla \cdot \hat{\eta}_i)\nabla\theta = \nabla \cdot (\hat{\eta}_i \otimes \nabla\theta) - \nabla|\nabla\theta|, \tag{19}$$

and subsequently to the conservation of linear momentum

$$\int_\Omega (\nabla \cdot \hat{\eta}_i)\nabla\theta = \vec{0}, \tag{20}$$

provided that the contribution from the domain boundary, $\partial\Omega$, vanishes.

4 DISCRETE FORMULATION

The construction of the numerical setting requires to preserve the geometric identities described above. Such geometric identities imply the conservation of either energy (first variation of area) or momentum (integral of the mean curvature vector).

The discrete setting is based on a finite volume, staggered, second order formulation as described in [18]. Such a framework provides with the basic operators of discrete vector calculus. The transport of the marker function is performed by using a high resolution scheme, typically the Superbee flux limiter as in the original CLS scheme [14]. Nonetheless, although included in [14], recompression has been disregarded for the sake of energy conservation [18].

Following the framework described in [18], discrete variables are arranged into vectors (e.g.: θ_c, k_c), and discrete differential operators are arranged as matrices (e.g., G, D). The vector subindex determines its arrangement, stating c for collocated (cells) and f for staggered (faces); e.g.: θ_c and $\hat{n}_c$ are collocated, while n_f is staggered. The hat symbol determines that the discrete variable exists for the n components of the original vector, being $n = 2$ in 2D and $n = 3$ in 3D; e.g.: $\hat{n}_c$ is located at the cell centers and contains n-components for every cell, while n_f is located at the faces and only contains the projection of the vector in the face-normal direction. The computation of θ and $\hat{\eta}_i$ is performed at the cell centers, by constructing second order approximations to equation (10).

$$\hat{n}_c = ||G_c\theta_c||_{L2}^{-1} G_c\theta_c \qquad n_f = N_F \Pi \hat{n}_c \qquad k_c = D n_f \tag{21}$$

where we do take the cell-wise modulus of the collocated gradient, $||G_c\theta_c||_{L2}$, by taking the standard L_2 norm of its components at each cell.

Next, we will summarize our present knowledge on energy conservation [18] and our current efforts towards momentum conservation. Details for the conservation of energy can be found in [18]. In the quest of momentum conservation, we try to preserve the discrete structures that already provide with energy conservation.

4.1 Energy

The conservation of energy relies on satisfying the first variation of area (6). To do so, we follow [18], which we sketch briefly. In the context of a staggered mesh, this implies taking the point-wise product of both the staggered velocity and the staggered curvature. However, curvature is naturally defined in equation (21) at the cells, while the need the staggered value. However, the use of linear interpolation schemes [14] does not result in energy conservation.

Nonetheless, to interpolate the curvature from the cells to the faces provides with an opportunity to satisfy energy conservation. In this regard, we proceed by introducing a new cell-to-face interpolator Υ, which is the cell-to-face curvature interpolator, and assess its construction in terms of discrete energy conservation.

The surface area is described in terms of the CSF method in equation (21). Introducing the more compact inner product notation, $(f, g) = \int_\Omega fgdV$, we obtain a discrete version of the first variation of area as:

$$\left(\mathsf{G}\frac{d\theta_\mathsf{c}}{dt}, \hat{\mathsf{n}}_\mathsf{f}\right) = (\mathsf{G}\theta_\mathsf{c}, \mathsf{u}_\mathsf{f} \odot \Upsilon \mathsf{k}_\mathsf{c}) \tag{22}$$

where $\odot$ corresponds with the element-wise product.

We then consider the discrete evolution of surface energy in terms of the transport of the marker function. This describes the time derivative of the discrete marker function.

$$\frac{d\theta_\mathsf{c}}{dt} = \mathsf{C}(\mathsf{u}_\mathsf{f})_\mathsf{c}\theta_\mathsf{c} \tag{23}$$

Due to the abrupt discontinuity of the marker function, the use of a high resolution scheme is in place. In particular, we use a Superbee flux limiter, as in the original transport equation of the CLS [14].

After rearranging equation (22) (see [18] for details), we arrive at the final condition for Υ:

$$\mathsf{C}(\mathsf{u}_\mathsf{f})_\mathsf{c}{\mathsf{u}_\mathsf{f}}^T = -\mathsf{D}\left(\mathsf{u}_\mathsf{f} \odot \Upsilon\right) \tag{24}$$

which relates the construction of the high resolution convective operator for θ_c, $\mathsf{C}(\mathsf{u}_\mathsf{f})_\mathsf{c}\mathsf{u}_\mathsf{f}$ with the the curvature interpolator Υ. By splitting the flux limiter into a symmetric and a skew-symmetric part [27], it can be shown that the face-to-cell curvature interpolator must be dual to the cell-to-face marker function interpolator [18]. In summary, the curvature interpolator must use as much downwind interpolation as upwind interpolation is used for θ_c. A graphical example can be seen in Figure 1, where Ψ stands for the high resolution interpolator.

4.2 Linear momentum

The conservation of linear momentum at discrete level turned out to be a very complex problem. In view of the identity (19) found in this work, there exists a straightforward way to preserve linear momentum. Namely, simply ignoring the gradient term, $\nabla|\nabla\theta|$, in the regularized continuous formulation. In this way, we just need to discretize the first term in the r.h.s. of Eq.(19), $\nabla \cdot (\hat{\eta}_i \otimes \nabla\theta)$, which is in divergence convective form; therefore, preserving the linear momentum. The term $\nabla|\nabla\theta|$ would be absorbed into the pressure field, i.e. $\pi = p + |\nabla\theta|$. However, doing so, the conservation of mechanical energy cannot be guaranteed any more. Notice that the method developed in [18], and briefly outlined in the previous section, relies on

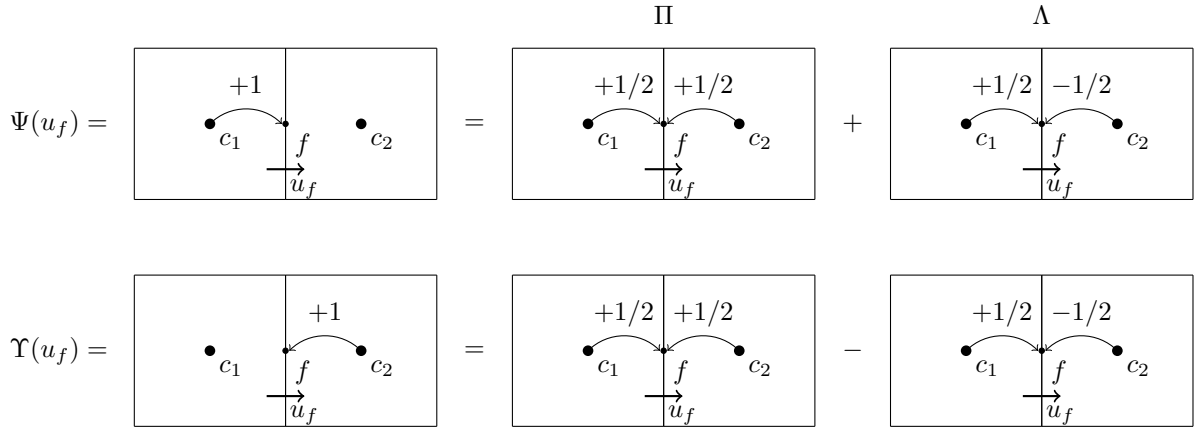

Figure 1: The curvature interpolator Υ is constructed in terms of the interpolation used in the construction of the fluxes at the faces of $\mathsf{C}(\mathsf{u_f})_\mathsf{c}$.

discretizing both the surface tension and the convective term in the transport equation of the marker function in a consistent way.

Hence, it seems that if we aim to preserve both mechanical energy and linear momentum, we need to mimic the mathematical properties that lead to the conservation of the linear momentum for the regularized formulation in Section 3.2. Likewise the continuous case, the cornerstone seems to be to preserve the orthogonality between the tensor $\nabla\hat{\eta}_i$ and the vector $\nabla\theta$ (see Eq. 18) at discrete level (for the sake of brevity details are omitted here). Very shortly, in 2D (3D extension is straightforward) we end up with the following discrete term

$$(\mathsf{M_F G}^x \hat{\mathsf{n}}_\mathsf{x}) \odot (\Pi \mathsf{g}_\mathsf{x}) + (\mathsf{M_F G}^y \hat{\mathsf{n}}_\mathsf{y}) \odot (\Pi \mathsf{g}_\mathsf{y}), \tag{25}$$

where $\mathsf{g_x}$ and $\mathsf{g_y}$ are the cell-centered gradients in x and y direction, $\hat{\mathsf{n}}_\mathsf{x}$ and $\hat{\mathsf{n}}_\mathsf{y}$ are the respective cell-centered (interface) normals and G^x and G^y represent the discrete cell-to-face gradient operator, G, projected into x and y directions. This expression resembles the continuous counterpart given in Eq.(18) and must be exactly zero to preserve linear momentum at discrete level. Several face-to-cell and cell-to-face interpolations are required to construct a numerical approximation. Current research plans are focused on finding appropriate relations between these discrete operators to guarantee that expression (25) vanishes.

5 RESULTS AND CONCLUSIONS

A typical example is presented for a bubble of diameter $R = 0.15$ placed at the center of a box $[1 \times 1 \times 1]$, which is represented by a mesh of $[96 \times 96 \times 96]$ cells. In the absence of gravity and viscosity, velocity should remain stagnant. Stretching the bubble by 20% in the $y-$axis, the problem turns into a multi-dimensional version of an (undamped) mass-spring system, which is meant to continuosly oscillate. Tests are performed for density ratios 1 and $1e-3$.

Considering linear perturbation theory for an ellipsoid, one can determine the oscillating period as [28]:

$$T = 2\pi\sqrt{\frac{R^3\left((s+1)\rho_1 + s\rho_0\right)}{\gamma s(s^2-1)(s+2)}} \tag{26}$$

being ρ_1 and ρ_0, the bubble and liquid densities, respectively.

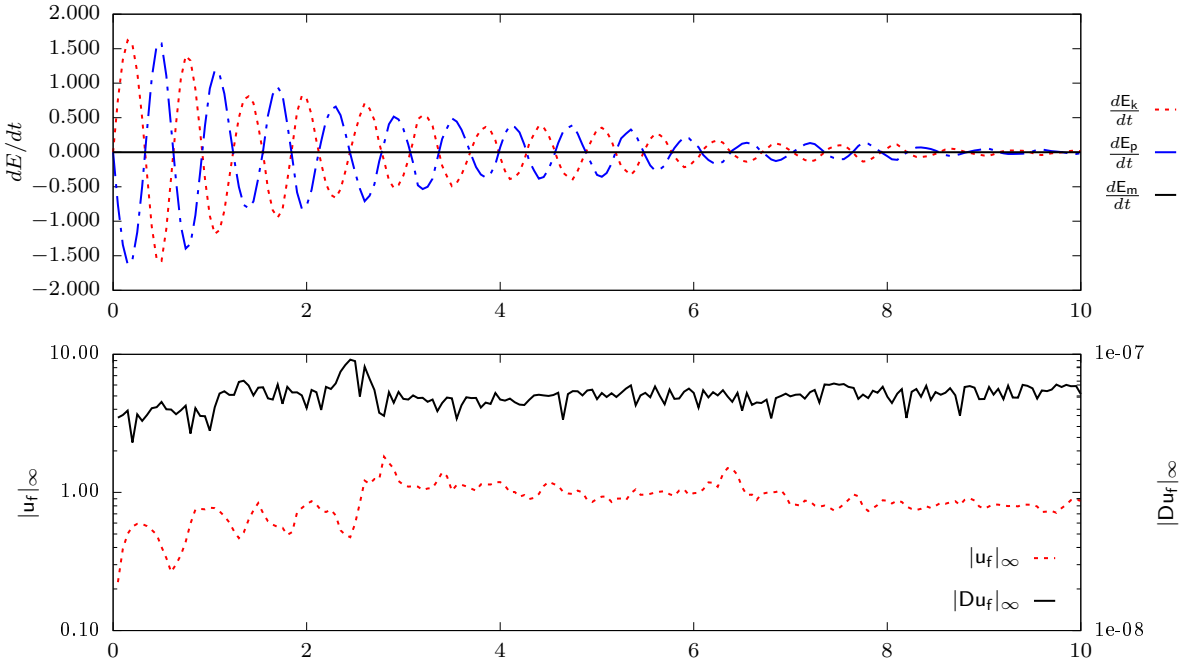

Figure 2: Flow metrics evolution for an ellipsoid for unit density ratio. Top: Energy evolution. Bottom: Evolution of $|u|_\infty$ and $|\mathsf{Du_f}|_\infty$.

Results show how the simulation of these cases does preserve the energy transfer exactly (up to an incompressible flow field), preserving both the physics of the problem as well as numerical stability. It can be observed, however, a damping in the amplitude of such energy transfers. Since there is no dissipation, this can only be attributed to an erroneous computation of the intensity of such transfers, i.e., the computation of the actual capillary force.

We assume that these errors are due to the lack of momentum conservation, which may lead to the production of inaccurate solutions, i.e.: incorrect re-distribution of elastic and kinetic energy. Eventually, the system evolves into a stagnant case, since all the energy that was available at the beginning of the simulation is eventually allocated as surface energy. As described above, the conservation of linear momentum in the capillary term is ongoing work.

Finally, we have exposed the relevance of the conservation of primary and secondary properties, delved into the mathematical identities behind them, and successfully brought them from the continuum to the regularized formulation. While we have partially succeed on bringing those to the discrete formulation, most remarkably energy, the development of a simultaneously preserving mass, momentum and energy scheme is still work in progress.

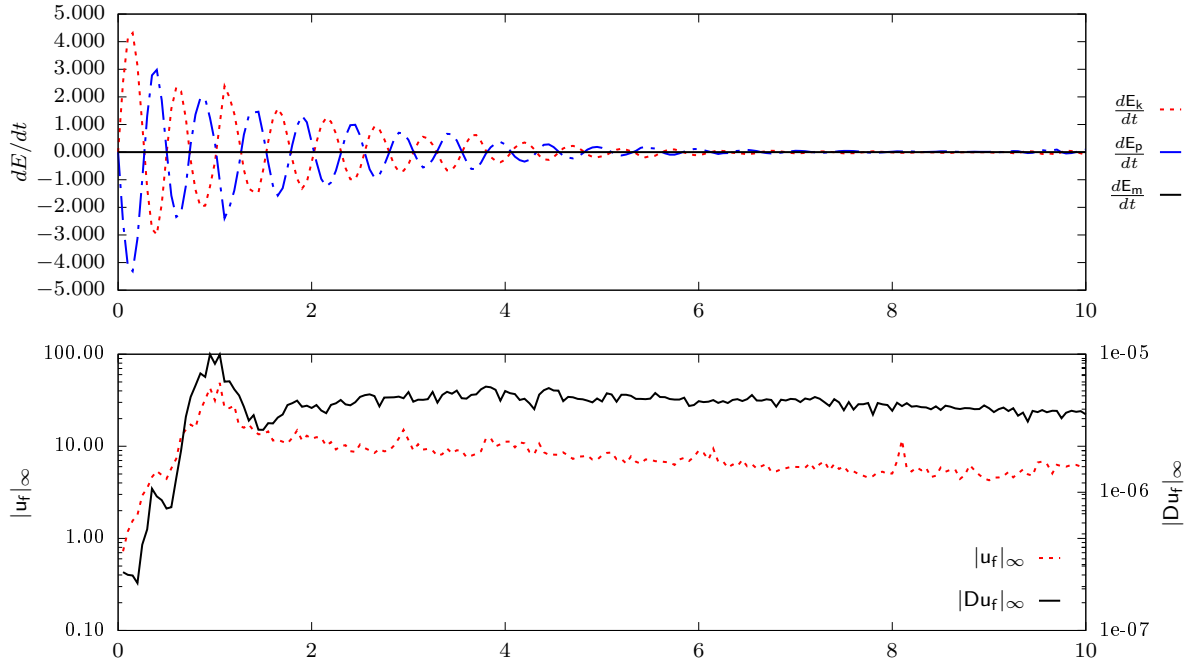

Figure 3: Flow metrics evolution for an ellipsoid for $\rho_1/\rho_0 = 10^{-3}$. Top: Energy evolution. Bottom: Evolution of $|u|_\infty$ and $|\mathsf{Du_f}|_\infty$.

ACKNOWLEDGEMENTS

We thank the Center for Information Technology of the University of Groningen for their support and for providing access to the Peregrine high performance computing cluster.

References

[1] N. K. Madavan, S. Deutsch, and C. L. Merkle. Physics of Fluids 27.2 (1984), 356–363. http://doi.org/10.1063/1.864620.

[2] M. Schludieter, S. Herres-Pawlis, U. Nieken, U. Tuttlies, and D. Bothe. Annual Review of Chemical and Biomolecular Engineering 12 (2021), 625–643. http://doi.org/10.1146/annurev-chembioeng-092220-100517.

[3] D. Lohse. Physical Review Fluids 3.11 (2018), 1–42. http://doi.org/10.1103/PhysRevFluids.3.110504.

[4] V. Spandan, R. Verzicco, and D. Lohse. Journal of Fluid Mechanics 849 (2018), R31–R313. http://doi.org/10.1017/jfm.2018.478.

[5] J. Hasslberger, M. Klein, and N. Chakraborty. Journal of Fluid Mechanics 857 (2018), 270–290. http://doi.org/10.1017/jfm.2018.750.

[6] F. Risso. Annual Review of Fluid Mechanics 50 (2018), 25–48. http://doi.org/10.1146/annurev-fluid-122316-045003.

[7] R. W. C. P. Verstappen and A. E. P. Veldman. Journal of Computational Physics 187.1 (2003), 343–368. http://doi.org/10.1016/S0021-9991(03)00126-8.

[8] F. X. Trias, O. Lehmkuhl, A. Oliva, C. D. Pérez-Segarra, and R. W. C. P. Verstappen. Journal of Computational Physics 258 (2014), 246–267. http://doi.org/10.1016/j.jcp.2013.10.031.

[9] S. Elghobashi. Annual Review of Fluid Mechanics 51 (2019), 217–244. http://doi.org/10.1146/annurev-fluid-010518-040401.

[10] S. Popinet. Annual Review of Fluid Mechanics 50.1 (2017), 49–75. http://doi.org/10.1146/annurev-fluid-122316-045034.

[11] E Trautner, J Hasslberger, T Trummler, P Cifani, R Verstappen, and M Klein. *13th International ERCOFTAC symposium on engineering, turbulence, modelling and measurements*. Rhodes, 2021.

[12] C. W. Hirt and B. D. Nichols. Journal of Computational Physics 39.1 (1981), 201–225. http://doi.org/10.1016/0021-9991(81)90145-5.

[13] D. M. Anderson, G. B. McFadden, and A. A. Wheeler. Annual Review of Fluid Mechanics 30.1 (1998), 139–165. http://doi.org/10.1146/annurev.fluid.30.1.139.

[14] E. Olsson and G. Kreiss. Journal of Computational Physics 210.1 (2005), 225–246. http://doi.org/10.1016/j.jcp.2005.04.007.

[15] D. Jacqmin. Journal of Computational Physics 155.1 (1999), 96–127. http://doi.org/10.1006/jcph.1999.6332.

[16] S. Mirjalili, C. B. Ivey, and A. Mani. Journal of Computational Physics 401 (2020), 109006. http://doi.org/10.1016/j.jcp.2019.109006.

[17] D. Fuster. Journal of Computational Physics 235 (2013), 114–128. http://doi.org/10.1016/j.jcp.2012.10.029.

[18] N. Valle, F. X. Trias, and J. Castro. Journal of Computational Physics 400 (2020), 108991. http://doi.org/10.1016/j.jcp.2019.108991.

[19] M. O. Abu-Al-Saud, S. Popinet, and H. A. Tchelepi. Journal of Computational Physics 371 (2018), 896–913. http://doi.org/10.1016/j.jcp.2018.02.022.

[20] S. Mirjalili, S. S. Jain, and M. S. Dodd. *Interface-capturing methods for two-phase flows: An overview and recent developments*. Tech. rep. Center for Turbulence Research, 2017.

[21] A. Marchand, J. H. Weijs, J. H. Snoeijer, and B. Andreotti. American Journal of Physics 79.10 (2011), 999–1008. http://doi.org/10.1119/1.3619866.

[22] R. W. C. P. Verstappen and A. E. P. Veldman. Journal of engineering mathematics 32 (1997), 143–159. http://doi.org/https://doi.org/10.1023/A:1004255329158.

[23] A. E. Veldman. Journal of Computational Physics 398 (2019), 108894. http://doi.org/10.1016/j.jcp.2019.108894.

[24] T. Frankel. *The Geometry of Physics*. 3rd ed. Cambridge: Cambridge University Press, 2012. DOI: 10.1017/CBO9781139061377.

[25] D. Blackmore and L. Ting. SIAM Review 27.4 (1985), 569–572. http://doi.org/10.2307/2031060.

[26] J. Brackbill, D. Kothe, and C Zemach. Journal of Computational Physics 100.2 (1992), 335–354. http://doi.org/10.1016/0021-9991(92)90240-Y.

[27] N. Valle, X. Álvarez-Farré, A. Gorobets, J. Castro, A. Oliva, and F. X. Trias. Computer Physics Communications (2021), 108230. http://doi.org/10.1016/j.cpc.2021.108230.

[28] S. H. Lamb. *Hydrodynamics*. New York, NY: Dover Publications, Inc., 1945, pp. 123–124.